Low-loss photonic device in Ge–Sb–S chalcogenide glass

Citation: Du, Qingyang et al. "Low-Loss Photonic Device in Ge–Sb–S Chalcogenide Glass." Optics Letters 41, 13 (June 2016): 3090-3093 © 2016 Optical Society of America

As Published: https://doi.org/10.1364/OL.41.003090

Publisher: Optical Society of America

Persistent URL: http://hdl.handle.net/1721.1/112647

Version: Author's final manuscript: final author's manuscript post peer review, without publisher's formatting or copy editing

Low Loss Photonic Device in Ge-Sb-S Chalcogenide Glass

QINGYANG DU[1], YIZHONG HUANG[1,2], JUNYING LI[1,3], DEREK KITA[1], JÉRÔME MICHON[1], HONGTAO LIN[1], LAN LI[1], SPENCER NOVAK[4,5], KATHLEEN RICHARDSON[4], WEI ZHANG[1,6], AND JUEJUN HU[1,*]

[1]*Department of Materials Science and Engineering, Massachusetts Institute of Technology, Cambridge MA, 02139*
[2]*Department of Electronic Engineering, Xiamen University, Xiamen 361005, China*
[3]*The Key Laboratory of Optoelectronic Technology & System, Education Ministry of China, Chongqing University, Chongqing 400044, China*
[4]*College of Opticsand Photonics, CREOL, Department of Materials Science and Engineering, University of Central Florida, Orlando, Florida 32816, USA*
[5]*now at Lightpath Technologies, Orlando, Florida 32816 USA*
[6]*Key Laboratory of Photoelectric Materials and Devices of Zhejiang Province, Ningbo University, Ningbo, Zhejiang 315211, China*
*Corresponding author: *hujuejun@mit.edu*

Received XX Month XXXX; revised XX Month, XXXX; accepted XX Month XXXX; posted XX Month XXXX (Doc. ID XXXXX); published XX Month XXXX

Low-loss waveguides constitute an important building block for integrated photonic systems. In this work, we investigated low-loss photonic device fabrication in $Ge_{23}Sb_7S_{70}$ chalcogenide glass using electron beam lithography followed by plasma dry etching. High-index-contrast waveguides with a low propagation loss of 0.5 dB/cm and micro-disk resonators with an intrinsic quality factor (Q-factor) of 1.2×10^6 were demonstrated. Both figures represent the best low loss results reported thus far in sub-micron single-mode chalcogenide glass devices.

OCIS codes: *(230.5750) Resonators; (160.2750) Glass and other amorphous materials(230.7370) Waveguides; (130.3120) Integrated optics devices; (130.2755) Glass waveguides.*

http://dx.doi.org/10.1364/OL.99.099999

Chalcogenide glasses (ChGs) are widely recognized as the material of choice for sensing, flexible substrate integration and all-optical signal processing due to their broad transparency window in the infrared region, low processing temperature, and high Kerr nonlinearity [1-5]. In addition, their high refractive indices enable small optical mode volume without suffering from excessive radiative loss. Nevertheless, unlike standard integrated photonic materials with well-established processing protocols such as silicon and silica, planar processing of ChGs remains much less mature despite their exceptional optical properties. Prior work has explored planar ChG photonic device fabrication using standard semiconductor microfabrication techniques such as plasma etching, wet etching [6], ion milling [7], nanoimprint [8, 9], and lift-off [10]. In particular, Madden *et al.* [11] demonstrated a remarkable low propagation loss of 0.05 dB/cm in large-core rib waveguides via fluorine plasma etching. Small-core single-mode strip waveguides, however, suffer from much higher loss due to the stronger optical modal overlap with rough waveguide sidewalls. The best reported result of 0.84 dB/cm was obtained recently by Chiles *et al.* [12] using plasma etching with a chlorine chemistry. We note that in both cases, the waveguide loss figures far exceed the intrinsic material attenuation in ChG materials, as Q-factors as high as 7.2×10^7, which corresponds to an optical loss of less than 0.002 dB/cm, have been reported in ChG microspheres [13]. It is apparent that optical scattering from waveguide sidewall roughness and possibly glass inhomogeneity [14] represent the dominant attenuation mechanism in the measured waveguide loss.

Our prior work had relied on UV photolithography for ChG microphotonic device fabrication, although large sidewall roughness (10-15 nm root mean square [15]) due to the limited feature resolution can compromise the resulting device performance. In this paper, we report a systematic study of low-loss ChG device processing using electron beam lithography coupled with reactive ion dry etching. Compared to UV photolithography, electron beam (e-beam) lithography is known to offer deep-sub-micron resolution and significantly reduced pattern edge roughness, and is therefore suited for low-loss, high-index-contrast ChG device processing. Both chlorine and fluorine etching gases are investigated, as both chemistries have been adopted for low-loss ChG device patterning [11, 12].

The ChG devices were fabricated on 6" silicon wafers with 3 μm thermally grown oxide coating (Silicon Quest International). A piranha clean was performed prior to film deposition to remove any organic residue from the wafer surface. Subsequently, $Ge_{23}Sb_7S_{70}$ (GSS) bulk glass prepared by conventional melt/quench protocols previously reported [16] was thermally evaporated onto the wafer to form a 450-nm-thick ChG film using established protocols [16].

We chose the GSS composition over the classical As_2S_3 or As_2Se_3 systems given the superior oxidation-resistance of GSS glass, whereas As_2S_3 or As_2Se_3 glasses are prone to surface oxidation [9]. The deposition rate was maintained at 15 Å/s. A 400-nm-thick ZEP-520A resist (ZEON Chemicals) layer was then spun onto the glass film and exposed by an Elionix ELS-F125 e-beam lithography tool using a beam current of 10 nA. The resist was then developed by immersing in ZED-N50 (ZEON Chemicals) for 1 minute to reveal the patterns.

Reactive ion etching was then carried out on a PlasmaTherm reactive ion etching (RIE) tool (PlasmaTherm Inc.). Both chlorine and fluorine chemistries were investigated. In both cases, the gas flow rate, chamber pressure, radio-frequency (RF) power and etching gas ratio (for the fluorine chemistry) were systematically varied to determine the optimal etching recipes which generate photonic devices with minimal loss (detailed results not shown). Table 1 summarizes the optimized etching parameters for both chemistries. Channel waveguides with cross-sectional dimensions of 800 nm × 450 nm were fabricated by etching through the entire GSS layer. After etching, remaining resists were stripped by soaking the sample in N-Methyl-2-pyrrolidone (NMP) for 2 hours and then sonicating for 30 seconds. The fluorine etched samples underwent an additional oxygen plasma treatment step to remove the fluorocarbon polymer deposited on the waveguide sidewalls formed during the plasma process.

Table I. Summary of the etching conditions for Chlorine chemistry and Fluorine chemistry

	Chlorine	*Fluorine*
Chemistry	Cl_2	CHF_3:CF_4 3:1
Gas flow rate (sccm)	24	45:15
Pressure (mTorr)	10	5
RF Power (W)	200	200

Figure 1 shows the top-view and cross-sectional SEM images of GSS waveguides prepared using the recipe listed in Table 1. As seen in Fig 1a, chlorine-etched waveguides feature a clean, residue-free morphology consistent with previous report [12]. However, the chlorine-etched waveguide sidewalls are encapsulated by a thin coating layer (the white lines on the waveguide edges shown in Fig. 1a) with a composition different from that of GSS, evidenced by the secondary electron image contrast in Fig. 1b. In some cases, the coating layer was also formed on the ZEP resist sidewalls, which upon resist removal resulted in a "bunny ear" geometry protruding on top of the waveguide (Fig. 1b). We performed X-ray Photoelectron Spectroscopy (XPS) titled beam analysis to ascertain the coating layer composition. In the experiment, a GSS grating sample was prepared using the same set of parameters used to etch the waveguide devices. Fig. 2a illustrates the XPS interrogation configuration: the grating duty cycle and height as well as the X-ray incident angle are chosen so that the X-ray beam pre-dominantly interacts with the grating line sidewalls (and top surface of grating lines to a much lesser extent) to exclude spurious signals from the substrate. Since XPS is a surface-sensitive technique with typical penetration depths less than 10 nm, the XPS spectrum shown in Fig. 2b represents the surface coating layer composition. The XPS result indicates that the coating contains Si, O, C (a common atmospheric contaminant routinely observed on samples exposed to ambient environment) and trace amount of F which is likely introduced from the etching chamber. Furthermore, the coating can be removed by rinsing the sample in dilute HF solutions. We therefore conclude that the coating layer mostly consists of silicon oxide. This is not surprising since the plasma etching chamber we used was located in a shared facility and was therefore routinely used for etching silicon compounds. In fact, similar silicon oxide coatings were identified on plasma etched III-V semiconductor nanostructures [17] for the same reason as we identified here.

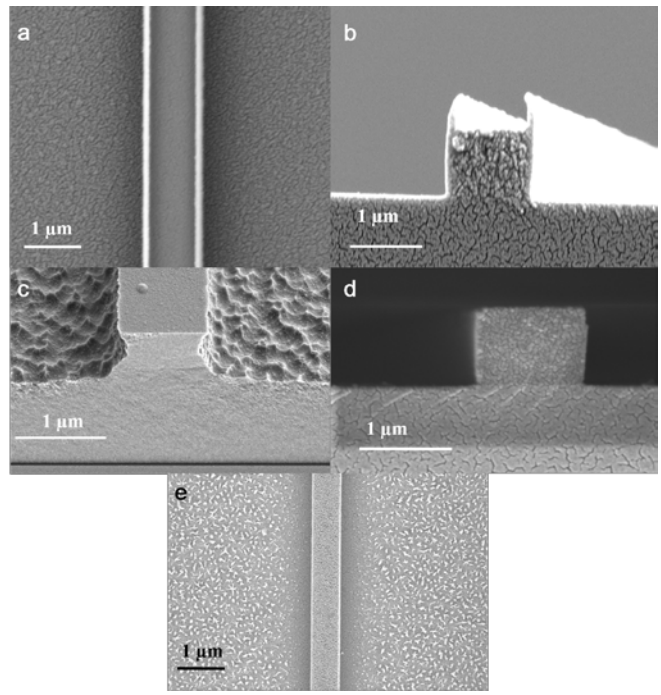

Fig. 1. SEM images of: a, b) chlorine-etched GSS waveguides with silicon oxide passivation coating; the grainy surface texture comes from gold coating applied to reduce electrostatic charging during SEM imaging; c) chlorine-etched GSS waveguide without silicon oxide passivation coating; d, e) fluorine-etched GSS waveguides.

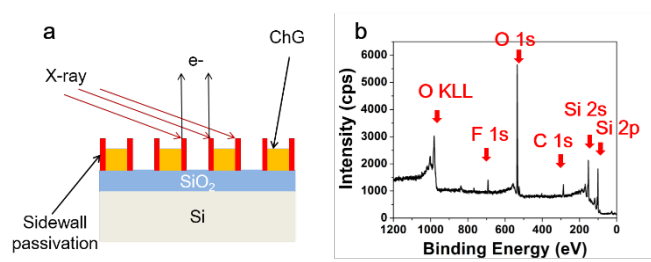

Fig. 2. a) Schematic diagram showing the XPS tilted beam analysis configuration. The grating has a 400 nm line width with 800 nm period. b) XPS spectrum showing the presence of Si and O, and trace amounts of C, F in the coating layer.

To further clarify the role of the silicon oxide coating in defining the etched structure geometry, we performed another set of plasma etching tests after thoroughly cleaning the etching chamber

immediately prior to chlorine etching, but otherwise followed identical experimental protocols. Severe undercut was observed in etched waveguides, which is accompanied with significant increase of sidewall roughness as shown in Fig. 1c. The result suggests that the silicon oxide coating which spontaneously forms during the plasma etching step is essential to minimizing radical chemical attack on the GSS pattern sidewalls and maintaining a vertical sidewall profile. This can be envisioned, as silicon oxide is known to be inert in a chlorine plasma.

Figure 1d and 1e show that fluorine etching similarly generates a nearly vertical sidewall profile. During the fluorine etch, carbon and fluorine radicals generated by the plasma react to form a fluorocarbon polymer passivation layer on the sidewall that prevents lateral etching. The fluorocarbon polymer coating also accounts for the residue observed on the etched surfaces at the two sides of the waveguide (Fig. 1d) formed by self-masking [18]. It is interesting to note that the vicinity of the waveguide is free of residues, likely due to shadowing effect. This phenomenon is useful to producing waveguide devices with smooth sidewalls and low optical loss.

Performance of the fabricated devices near 1550 nm wavelength was evaluated using a fiber end fire coupling method on a LUNA Technology laser with built-in Optical Vector Analyzer. To quantitatively assess propagation loss, micro-ring and micro-disk resonators were fabricated by both chlorine and fluorine etching. Optical micrographs of the fabricated resonator samples are shown in Fig. 3a and 3b. All resonators are 50 µm in radius. Both the micro-ring and the coupling bus waveguides have cross-sectional dimensions of 800 nm × 450 nm. Fig 3c plots a representative transmission spectrum of the micro-ring resonator. The best micro-ring resonator performance is obtained in devices etched by the fluorine chemistry, which yields an intrinsic Q factor of 750,000. The waveguide propagation loss α (in cm^{-1}) is calculated using Eq. 1:

$$\alpha = \frac{2\pi n_g}{Q\lambda_r} \quad \textbf{(1)}$$

where λ_r denotes the resonant wavelength, and n_g represents the group index. The group index is inferred from the Free Spectral Range (FSR) using Eq. 2

$$n_g = \frac{\lambda_r^2}{L \times FSR} \quad \textbf{(2)}$$

to be 2.30, where L is the round trip length of the resonator. Eq. 1 gives a waveguide propagation loss of 0.5 dB/cm. To the best of our knowledge, this value represents the lowest loss figure reported in sub-micron single-mode ChG channel waveguides.

Micro-disk resonators prepared using the same etching protocols yield high quality factors of 10^6 (not shown) for chlorine etched samples and 1.2×10^6 (Fig. 3f) for fluorine etched samples, the highest Q-factors in planar ChG optical devices [12, 19-23]. Although both etching chemistries are capable of producing high Q-factors, fluorine etching is preferred over chlorine etching in our case since sidewall passivation using silicon oxide in the case of chlorine etching requires deliberate introduction of trace silica contaminants into the etching chamber, which is far less reproducible compared to fluorocarbon polymer formation during fluorine etching.

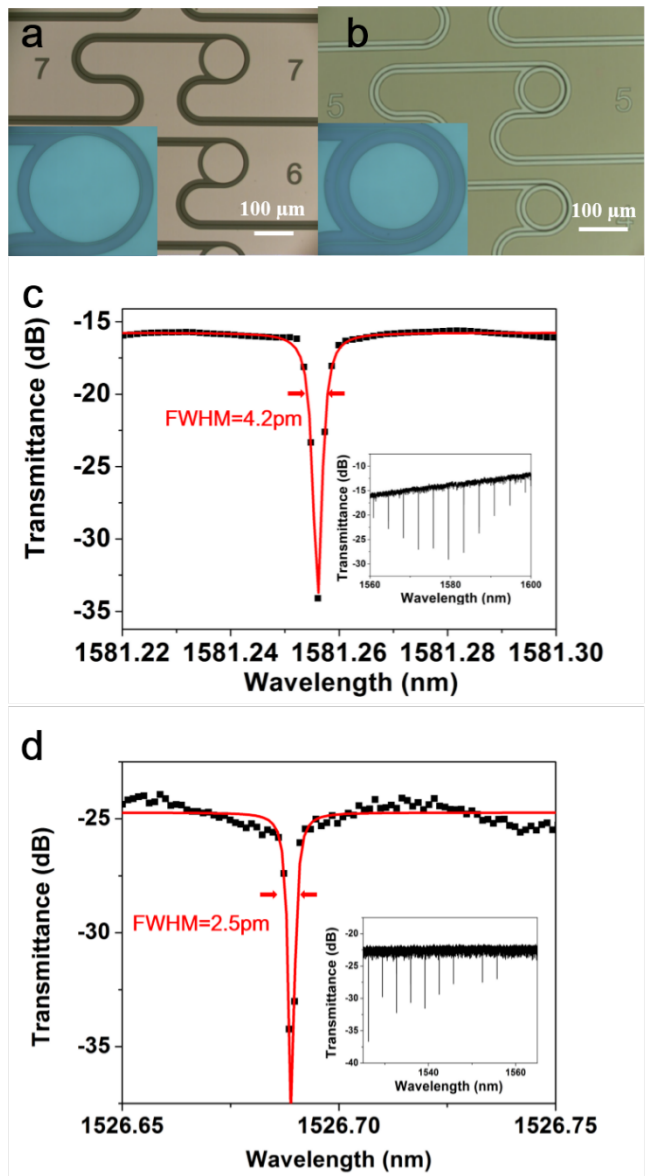

Fig. 3. Optical microscope images of fabricated a) micro-disk and b) micro-ring resonators. c-d) Transmission spectra of c) micro-ring resonator; and d) micro-disk resonator etched using the fluorine chemistry. The red curves are Lorentzian fit of the spectra.

To quantify the roughness scattering contribution to optical loss, sidewall roughness of the waveguides was determined from high magnification SEM images using the imaging processing software ImageJ. In the example shown in Fig. 4, the waveguide edge profile, represented by a function f(z), was extracted from the image using grayscale analysis. The roughness metrics were subsequently evaluated following procedures described in Ref. [24] and the results were averaged over multiple waveguides. Specifically, the autocorrelation function of the waveguide sidewall roughness is calculated using:

$$R(u) = \langle f(z) \cdot f(z+u) \rangle \quad \textbf{(3)}$$

where the brackets represent ensemble average. The roughness power spectral density (PSD) function is the Fourier transform of R(u). The PSD function is plotted in Fig. 4c and a root-mean-square

(RMS) roughness of (2.4 ± 0.2) nm for fluorine etched waveguides is obtained from the analysis. Fig. 4c further suggests that the roughness distribution does not comply with either the exponential model or the white noise model. Following the 3-D volume current method in Ref. [24], we estimate that sidewall roughness scattering contributes approximately 0.2 dB/cm optical loss.

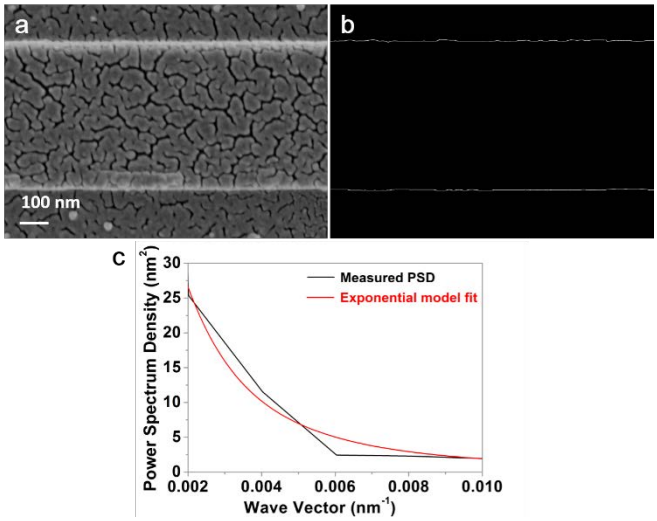

Figure 4. Waveguide sidewall roughness analysis example: a) SEM top-view image of a fluorine etched waveguide; the grainy surface texture comes from gold coating applied to reduce electrostatic charging during SEM imaging. b) Waveguide edge extracted from the SEM image. c) PSD function of sidewall roughness (black line). The red line represents exponential model fit.

In summary, we have demonstrated low-loss GSS photonic device fabrication using electron beam lithography and plasma etching. Optimized chlorine and fluorine etching chemistries are both capable of producing vertical sidewalls and low-loss devices. For fluorine etching, fluorocarbon polymers develop during deposition and provide sidewall passivation, whereas non-intentionally introduced silicon oxide impurities are the primary passivation agent in chlorine etching. A low propagation loss of 0.5 dB/cm and a high Q-factor of 1.2 million were obtained in sub-micron single-mode waveguides and micro-disk resonators patterned using fluorine etching, respectively. These values represent the best low loss performance reported to date in planar chalcogenide glass devices.

Funding. This work is supported by NSF awards 1506605 and 1453218, NNSA grant DE-NA0002509, and DTRA grant HDTRA1-13-1-0001.

Acknowledgment. The authors also acknowledge material characterization and fabrication facility support by MIT Center of Materials Science & Engineering (CMSE) and the Microsystems Technology Laboratories.

References

1. B. J. Eggleton, B. Luther-Davies, and K. Richardson, Nat. Photonics **5**, 141(2011).
2. V. Singh, P. T. Lin, N. Patel, H. Lin, L. Li, Y. Zou, F. Deng, C. Ni, J. Hu, and J. Giammarco, Sci. Technol. Adv. Mater. **15**, 014603 (2014).
3. J. Hu, L. Li, H. Lin, Y. Zou, Q. Du, C. Smith, S. Novak, K. Richardson, and J. D. Musgraves, Am. Ceram. Soc. Bull. **94**, 24 (2015).
4. L. Li, H. Lin, S. Qiao, Y. Zou, S. Danto, K. Richardson, J. D. Musgraves, N. Lu, and J. Hu, Nat. Photonics **8**, 643 (2014).
5. M.-L. Anne, J. Keirsse, V. Nazabal, K. Hyodo, S. Inoue, C. Boussard-Pledel, H. Lhermite, J. Charrier, K. Yanakata, and O. Loreal, Sensors **9**, 7398 (2009).
6. T. V. Galstyan, J. Viens, A. Villeneuve, K. Richardson, and M. Duguay, J. Lightwave Technol. **15**, 1343 (1997).
7. Y. Ruan, W. Li, R. Jarvis, N. Madsen, A. Rode, and B. Luther-Davies, Opt. Express **12**, 5140 (2004).
8. T. Han, S. Madden, D. Bulla, and B. Luther-Davies, Opt. Express **18**, 19286 (2010).
9. Y. Zou, L. Moreel, L. Savelli, H. Lin, J. Zhou, L. Li, S. Danto, J. D. Musgraves, K. Richardson, K. Dobson, R. Birkmire, and J. Hu, Adv. Opt. Mater. **2**, 759 (2014).
10. J. Hu, N.-N. Feng, N. Carlie, L. Petit, J. Wang, A. Agarwal, K. Richardson, and L. Kimerling, Opt. Express **15**, 14566 (2007).
11. S. Madden, D.-Y. Choi, D. Bulla, A. V. Rode, B. Luther-Davies, V. G. Ta'eed, M. Pelusi, and B. J. Eggleton, Opt. Express **15**, 14414 (2007).
12. J. Chiles, M. Malinowski, A. Rao, S. Novak, K. Richardson, and S. Fathpour, Appl. Phys. Lett. **106**, 111110 (2015).
13. F. Vanier, M. Rochette, N. Godbout, and Y.-A. Peter, Opt. Lett. **38**, 4966 (2013).
14. R. Wang, A. V. Rode, S. Madden, C. Zha, R. Jarvis, and B. Luther-Davies, J. Non-Cryst. Solids. **353**, 950 (2007).
15. J. Hu, N.-N. Feng, N. Carlie, L. Petit, A. Agarwal, K. Richardson, and L. Kimerling, Opt. Express **18**, 1469 (2010).
16. J. Hu, V. Tarasov, A. Agarwal, L. Kimerling, N. Carlie, L. Petit, and K. Richardson, Opt. Express **15**, 2307 (2007).
17. S. Bouchoule, R. Chanson, A. Pageau, E. Cambril, S. Guilet, A. Rhallabi, and C. Cardinaud, J. Vac. Sci. Technol., A, **33**, 05E124 (2015).
18. D.-Y. Choi, S. Maden, A. Rode, R. Wang, and B. Luther-Davies, J. Non-Cryst. Solids. **354**, 3179 (2008).
19. S. Levy, M. Klebanov, and A. Zadok, Photonics Research **3**, 63-67 (2015).
20. X. Gai, B. Luther-Davies, and T. P. White, Opt. Express **20**, 15503 (2012).
21. P. Ma, D.-Y. Choi, Y. Yu, Z. Yang, K. Vu, T. Nguyen, A. Mitchell, B. Luther-Davies, and S. Madden, Opt. Express **23**, 19969 (2015).
22. Y. Zou, D. Zhang, H. Lin, L. Li, L. Moreel, J. Zhou, Q. Du, O. Ogbuu, S. Danto, J. D. Musgraves, K. Richardson, K. Dobson, R. Birkmire, and J. Hu, Adv. Opt. Mater. **2**, 478-486 (2014).
23. H. Lin, L. Li, Y. Zou, S. Danto, J. D. Musgraves, K. Richardson, S. Kozacik, M. Murakowski, D. Prather, P. Lin, V. Singh, A. Agarwal, L. C. Kimerling, and J. Hu, Opt. Lett. **38**, 1470 (2013).
24. T. Barwicz, and H. A. Haus, J. Lightwave Technol. **23**, 2719 (2005).

1. B. J. Eggleton, B. Luther-Davies, and K. Richardson, "Chalcogenide photonics," Nature photonics **5**, 141-148 (2011).

2. V. Singh, P. T. Lin, N. Patel, H. Lin, L. Li, Y. Zou, F. Deng, C. Ni, J. Hu, and J. Giammarco, "Mid-infrared materials and devices on a Si platform for optical sensing," Science and Technology of Advanced Materials **15**, 014603 (2014).

3. J. Hu, L. Li, H. Lin, Y. Zou, Q. Du, C. Smith, S. Novak, K. Richardson, and J. D. Musgraves, "Chalcogenide glass microphotonics: Stepping into the spotlight," American Ceramic Society Bulletin **94**, 24-29 (2015).

4. L. Li, H. Lin, S. Qiao, Y. Zou, S. Danto, K. Richardson, J. D. Musgraves, N. Lu, and J. Hu, "Integrated flexible chalcogenide glass photonic devices," Nature Photonics **8**, 643-649 (2014).

5. M.-L. Anne, J. Keirsse, V. Nazabal, K. Hyodo, S. Inoue, C. Boussard-Pledel, H. Lhermite, J. Charrier, K. Yanakata, and O. Loreal, "Chalcogenide glass optical waveguides for infrared biosensing," Sensors **9**, 7398-7411 (2009).

6. T. V. Galstyan, J. Viens, A. Villeneuve, K. Richardson, and M. Duguay, "Photoinduced self-developing relief gratings in thin film chalcogenide As2S3 glasses," IEEE Journal of Lightwave Technology **15**, 1343-1347 (1997).

7. Y. Ruan, W. Li, R. Jarvis, N. Madsen, A. Rode, and B. Luther-Davies, "Fabrication and characterization of low loss rib chalcogenide waveguides made by dry etching," Optics express **12**, 5140-5145 (2004).

8. T. Han, S. Madden, D. Bulla, and B. Luther-Davies, "Low loss Chalcogenide glass waveguides by thermal nano-imprint lithography," Optics express **18**, 19286-19291 (2010).

9. Y. Zou, L. Moreel, H. Lin, J. Zhou, L. Li, S. Danto, J. D. Musgraves, E. Koontz, K. Richardson, and K. D. Dobson, "Solution Processing and Resist-Free Nanoimprint Fabrication of Thin Film Chalcogenide Glass Devices: Inorganic–Organic Hybrid Photonic Integration," Advanced Optical Materials **2**, 759-764 (2014).

10. J. Hu, N.-N. Feng, N. Carlie, L. Petit, J. Wang, A. Agarwal, K. Richardson, and L. Kimerling, "Low-loss high-index-contrast planar waveguides with graded-index cladding layers," Optics express **15**, 14566-14572 (2007).

11. S. Madden, D.-Y. Choi, D. Bulla, A. V. Rode, B. Luther-Davies, V. G. Ta'eed, M. Pelusi, and B. J. Eggleton, "Long, low loss etched As 2 S 3 chalcogenide waveguides for all-optical signal regeneration," Optics express **15**, 14414-14421 (2007).

12. J. Chiles, M. Malinowski, A. Rao, S. Novak, K. Richardson, and S. Fathpour, "Low-loss, submicron chalcogenide integrated photonics with chlorine plasma etching," Applied Physics Letters **106**, 111110 (2015).

13. F. Vanier, M. Rochette, N. Godbout, and Y.-A. Peter, "Raman lasing in As 2 S 3 high-Q whispering gallery mode resonators," Optics letters **38**, 4966-4969 (2013).

14. R. Wang, A. V. Rode, S. Madden, C. Zha, R. Jarvis, and B. Luther-Davies, "Structural relaxation and optical properties in amorphous Ge 33 As 12 Se 55 films," Journal of Non-Crystalline Solids **353**, 950-952 (2007).

15. J. Hu, N.-N. Feng, N. Carlie, L. Petit, A. Agarwal, K. Richardson, and L. Kimerling, "Optical loss reduction in high-index-contrast chalcogenide glass waveguides via thermal reflow," Optics express **18**, 1469-1478 (2010).

16. J. Hu, V. Tarasov, A. Agarwal, L. Kimerling, N. Carlie, L. Petit, and K. Richardson, "Fabrication and testing of planar chalcogenide waveguide integrated microfluidic sensor," Optics Express **15**, 2307-2314 (2007).

17. S. Bouchoule, R. Chanson, A. Pageau, E. Cambril, S. Guilet, A. Rhallabi, and C. Cardinaud, "Surface chemistry of InP ridge structures etched in Cl2-based plasma analyzed with angular XPS," Journal of Vacuum Science & Technology A **33**, 05E124 (2015).

18. D.-Y. Choi, S. Maden, A. Rode, R. Wang, and B. Luther-Davies, "Plasma etching of As 2 S 3 films for optical waveguides," Journal of Non-Crystalline Solids **354**, 3179-3183 (2008).

19. S. Levy, M. Klebanov, and A. Zadok, "High-Q ring resonators directly written in As 2 S 3 chalcogenide glass films," Photonics Research **3**, 63-67 (2015).

20. X. Gai, B. Luther-Davies, and T. P. White, "Photonic crystal nanocavities fabricated from chalcogenide glass fully embedded in an index-matched cladding with a high Q-factor (> 750,000)," Optics express **20**, 15503-15515 (2012).

21. P. Ma, D.-Y. Choi, Y. Yu, Z. Yang, K. Vu, T. Nguyen, A. Mitchell, B. Luther-Davies, and S. Madden, "High Q factor chalcogenide ring resonators for cavity-enhanced MIR spectroscopic sensing," Optics express **23**, 19969-19979 (2015).

22. Y. Zou, D. Zhang, H. Lin, L. Li, L. Moreel, J. Zhou, Q. Du, O. Ogbuu, S. Danto, and J. D. Musgraves, "High-Performance, High-Index-Contrast Chalcogenide Glass Photonics on Silicon and Unconventional Non-planar Substrates," Advanced Optical Materials **2**, 478-486 (2014).

23. H. Lin, L. Li, Y. Zou, S. Danto, J. D. Musgraves, K. Richardson, S. Kozacik, M. Murakowski, D. Prather, and P. T. Lin, "Demonstration of high-Q mid-infrared chalcogenide glass-on-silicon resonators," Optics letters **38**, 1470-1472 (2013).

24. T. Barwicz, and H. A. Haus, "Three-dimensional analysis of scattering losses due to sidewall roughness in microphotonic waveguides," Lightwave Technology, Journal of **23**, 2719-2732 (2005).